Physics in Medicine & Biology

NOTE

Performance of a new accelerating-electrode-equipped fast-time-response PMT coupled with fast LGSO

IOP Publishing Phys. Med. Biol. 63 (2018) 05NT03 (8pp) https://doi.org/10.1088/1361-6560/aaad20

Physics in Medicine & Biology

IPEM Institute of Physics and Engineering in Medicine

NOTE

Performance of a new accelerating-electrode-equipped fast-time-response PMT coupled with fast LGSO

Seungeun Lee[1,2], **Min Sun Lee**[2,3], **Jun Yeon Won**[1,2] **and Jae Sung Lee**[1,2,3,4]

[1] Department of Biomedical Sciences, College of Medicine, Seoul National University, Seoul 03080, Republic of Korea
[2] Department of Nuclear Medicine, College of Medicine, Seoul National University, Seoul 03080, Republic of Korea
[3] Interdisciplinary Program in Radiation Applied Life Science, Seoul National University, Seoul 03080, Republic of Korea
[4] Institute of Radiation Medicine, Medical Research Center, Seoul National University College of Medicine, Seoul 03080, Republic of Korea

E-mail: jaes@snu.ac.kr

RECEIVED
12 October 2017

REVISED
31 January 2018

ACCEPTED FOR PUBLICATION
6 February 2018

PUBLISHED
2 March 2018

Keywords: photomultiplier tube, time resolution, transit time jitter

Abstract

In this study, we measured the performance of a newly developed Hamamatsu Photonics R13478 photomultiplier tube (PMT) and compared the results with those of an existing R9800 PMT. In R13478, an accelerating electrode is placed between the focusing electrode and first dynode for time resolution improvement through reduced transit time jitter. We investigated the time resolution dependence on the supply voltage and time pickoff method for R13478 and R9800 PMTs, each coupled with a $2.9 \times 2.9 \times 20\,mm^3$ fast LGSO:Ce (0.025 mol%) crystal. In addition, we measured the PMT time resolutions coupled with the crystals in edge and laid positions to determine the effects of the reduced position dependence of transit time in R13478. R13478 exhibited a better time performance than R9800 in various ways. The rise time of R13478 for our experimental setup was 1.54 ns, 100 ps shorter than that of R9800 because of the reduced transit time. Further, R13478 achieved a 169 ps single time resolution at the recommended supply voltage, while this value was 187 ps for R9800. The time resolution of R13478 was also significantly better for a low time pickoff threshold level and a high supplied voltage, which are conditions vulnerable to transit time jitter and noise, respectively. A considerable difference in time resolution was observed for the laid position (R13478: 144 ps; R9800: 167 ps), indicating that the accelerating electrode reduced spatial transit time difference. Overall, we showed the effects of the differentiated characteristics of R13478 PMT compared with R9800 and confirmed its excellent time performance. We suggest use of this device as a photodetector effective for fast timing applications such as time-of-flight positron emission tomography.

1. Introduction

Precise measurement of the radiation arrival time is critical for implementation of time-of-flight (TOF) technique in a positron emission tomography (PET) system, which yields improved lesion detection power (El Fakhri *et al* 2011, Karp *et al* 2008). In TOF PET, the line-of-response (LOR) is replaced by the segment-of-response (SOR), which is the LOR weighted based on the time difference of a pair of 511 keV annihilation photons converted to spatial information of the positron source (Mullani *et al* 1981, Tomitani 1981). Thus, timing uncertainties in radiation detection induce spatial uncertainties regarding source position, eventually lengthening the SORs. As excellent time resolution of PET system can yield direct improvement in the signal-to-noise ratio, this relationship emphasizes the important role of fast photodetectors. To date, various strategies to enhance time performance so as to maximize the efficiency of TOF technique have been explored (Conti 2011a, 2011b).

The most stable and established photodetector in PET is the photomultiplier tube (PMT). Because of its excellent intrinsic noise properties, the PMT has less dependence on the surrounding environment, including

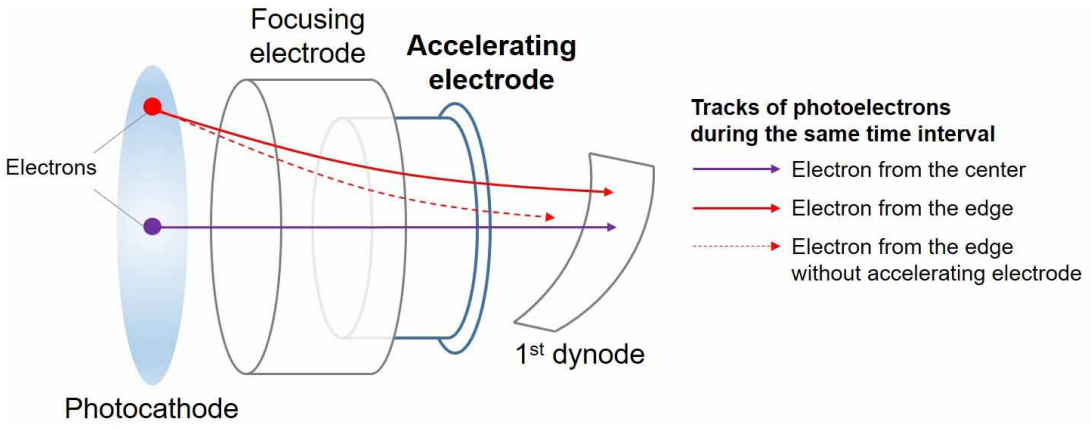

Figure 1. Effect of accelerating electrode on electron trajectories.

the temperature, than solid-state photodetectors (Adamo *et al* 2014). Other advantages of the PMT include radiation hardness and low output capacitance. Recent advances in metal-package multi-anode PMT technology have enabled the development of high-spatial-resolution PET detectors and systems with TOF measurement capability (Krishnamoorthy *et al* 2014, Ko and Lee 2015, Son *et al* 2016). However, the main limitation impeding the use of multi-anode PMTs is their higher cost compared to single-anode round-type PMTs, which are more suitable for mass production. Fast round-type PMTs equipped with 7–8 dynodes, which is less than 10–12 dynodes implemented in general PMTs, yield good time resolutions. The small number of dynodes reduces both the transit time and the transit time jitter which are the critical factors determining time performance of PMTs (Moses and Ullisch 2006, Moses 2007, Szczesniak *et al* 2007, Conti 2011b). In a previous study, round PMTs were coupled with $4 \times 4 \times 10\,\text{mm}^3$ lutetium yttrium orthosilicate (LYSO) crystals, yielding 200 ps single time resolution (Ito *et al* 2013).

The intrinsic transit time jitter of a PMT (σ_{PMT}) is composed of three factors: (1) the transit time variance due to different velocities of photoelectrons (σ_1^2); (2) the transit time variance due to different photoelectron emission positions at the photocathode (σ_2^2); and (3) the transit time variance arising when electrons travel between dynodes (σ_3^2). Therefore, the overall transit time variance in a PMT (σ_{PMT}^2) may be expressed with using these factors as follows (Moszyński and Vacher 1977):

$$\sigma_{\text{PMT}}^2 = \sigma_1^2 + \sigma_2^2 + \sigma_3^2. \quad (1)$$

One new approach to reducing transit time jitter σ_{PMT} is to use an additional electrode, named accelerating electrode (figure 1). This electrode is placed between the focusing electrode and first dynode, and is electrically connected to the last dynode to create a high electric potential. The accelerating electrode is expected to have two major effects. First, it can reduce σ_1^2. Photoelectrons are emitted with various initial velocities when scintillation lights arrive at the photocathode. By shortening the transit times via acceleration, the accelerating electrode reduces these variations in transit times. Second, σ_2^2 can also be reduced by the presence of the accelerating electrode, as this variance results from spatial transit time differences. In conventional PMTs, electrons emitted from the edge of the photocathode experience lower acceleration than those at the center, because the electric field is weaker at the edge. This causes variations in photoelectron traveling times from the photocathode to the first dynode, depending on emission position at the photocathode. The accelerating electrode can reduce these effects by generating an additional electric field near the edge, thereby harmonizing the transit times of the photoelectrons regardless of their origin.

In this study, we evaluated the physical performance of the R13478 (Hamamatsu Photonics K. K., Japan) PMT, which is a new one-inch round-type fast PMT equipped with an accelerating electrode and eight dynodes, when coupled with a next-generation fast cerium-doped lutetium gadolinium oxyorthosilicate (LGSO:Ce (0.025 mol%)) scintillation crystal. The performance of this PMT was compared with that of a Hamamatsu R9800 PMT, which has many similarities to R13478 but does not contain an accelerating electrode.

2. Materials and methods

2.1. PMTs and scintillators

A comparison of the specifications for the R13478 and R9800 PMTs, as provided by Hamamatsu Photonics, is given in table 1. R13478 and R9800 have the same size, photocathode material, and number of dynodes. The gain and typical anode dark current of R13478 are lower than those of R9800. The recommended supply voltages for operation are 1500 and 1300 V for R13478 and R9800, respectively. The transit time jitter of R13478 is 130 ps,

Table 1. PMT specifications provided by Hamamatsu Photonics.

PMT type	R13478	R9800
Recommended supply voltage (V)	1500	1300
Maximum supply voltage (V)	1750	1500
Rise time (ns)	0.9	1.0
Transit time (ns)	9.1	11
Transit time jitter (FWHM) (ps)	130	270
Gain	5.3×10^5	1.1×10^6
Anode dark current (nA)	3	5
Photocathode material	Bialkali	Bialkali
Dimension (mm)	⌀25.4	⌀25.4
Effective area (mm)	⌀22	⌀22
# of dynode stages	8	8
Accelerating electrode	Yes	No

FWHM: full width at half maximum.

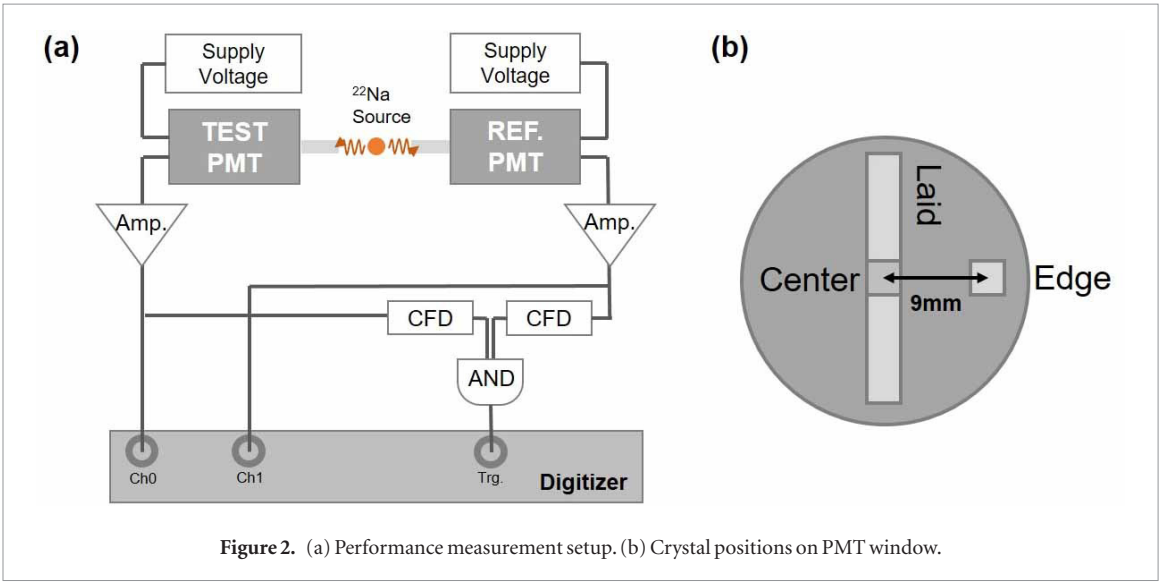

Figure 2. (a) Performance measurement setup. (b) Crystal positions on PMT window.

which is less than half that of R9800. The most remarkable difference between R13478 and R9800 is the presence of the accelerating electrode in the former.

As previously mentioned, we used a pair of fast LGSO:Ce (0.025 mol%) scintillation crystals to compare R13478 and R9800 PMTs. It is regarded as a good candidate material for next generation TOF PET crystals because of its advantages with regard to rise time, light output and high detection efficiency, when the optimized cerium concentration is implemented (Cates and Levin 2016). The crystal size was $2.9 \times 2.9 \times 20\,\text{mm}^3$ and the surfaces were chemically etched. Five crystal faces were wrapped with two layers of enhanced specular reflector (3M, USA) film. Single LGSO crystals were optically coupled to the PMT windows using optical grease (BC-630, Saint Gobain, France).

2.2. Data acquisition setup

Four R13478 and four R9800 PMTs were tested and the results of each PMT type were averaged in total for comparison. *P*-values were obtained by *t*-test. We used one of the R9800 PMTs with 1300 V supplied as a reference detector for the coincidence resolving time measurements, and its single time resolution was 186 ps. As shown in figure 2(a), test and reference PMT blocks were aligned facing each other with a ^{22}Na point source placed between them.

One of the branched pulses from both the reference and test PMTs was passed through CFD and AND modules for trigger and coincidence discrimination, respectively. In each case, more than 0.2 M coincidence events were sampled. We measured the performances of R13478 and R9800 for supply voltages of 1300–1700 V and 1100–1700 V, respectively, in 100 V intervals. Note that the recommended maximum supply voltage of R9800 is 1500 V, but higher voltages were supplied for fair comparison. In this measurement, the crystals were coupled to the centers of the PMT windows as shown in figures 2(a) and (b).

We tested two additional coupling positions of the same LGSO crystals (figure 2(b)) with the recommended supply voltages. First, the crystal was coupled at the edge of the test PMT window at a distance of 9 mm from

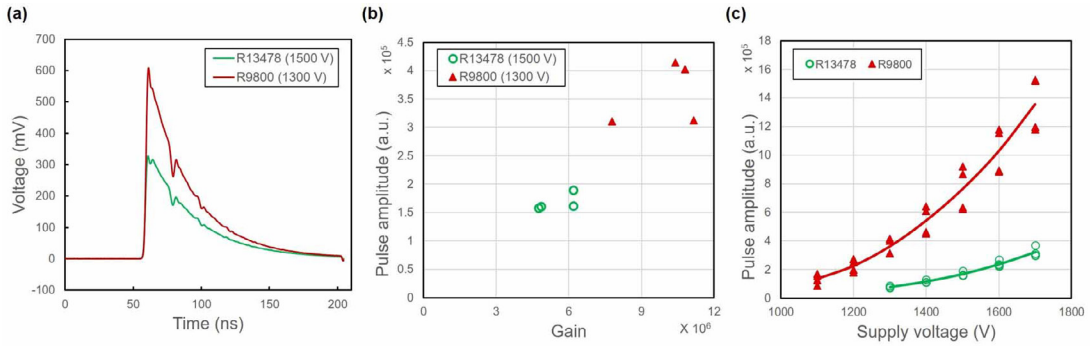

Figure 3. (a) Averaged pulse shapes of R13478 and R9800. (b) Pulse amplitude dependence on gain. The gain was calculated as (anode luminous sensitivity/cathode luminous sensitivity) × blue sensitivity index provided in the PMT data sheets. (c) Pulse amplitude dependence on supply voltage. An interactive version of this figure is available.

the center. Second, to widen the electron emitting area of the photocathode in order to investigate the effects of reduced spatial inhomogeneity for the transit time using the accelerating electrode, the side surface of the crystal ($2.9 \times 20\,\mathrm{mm}^2$) was laid down on the PMT window. To uniformly irradiate the laid crystal, the test detector was placed 15 cm from the reference detector with the point source attached.

The output pulses were sampled by a DRS4-based waveform digitizer (DT5742; CAEN, Italy) with a 5 GHz sampling rate and 12-bit sampling resolution. Because of its finite sampling resolution, a digitizer has an intrinsic quantization error that induces uncertainties in the time-stamp generation of the pulse arrivals. This is especially significant when the pulse amplitude is small, and can lead to unfair comparison of the time resolutions. Therefore, we adjusted the gain of the amplifier to keep the 511 keV photopeak amplitude similar for the measurements performed at different voltages.

2.3. Pulse processing and data analysis

We measured the energy and time resolutions of each configuration using the pulses sampled by the digitizer. The energy of each pulse was measured by integrating values sampled for a 160 ns time duration. From the energy histogram, the energy resolution (%) was estimated based on the full width at half maximum (FWHM) of the Gaussian fit of the 511 keV peak.

Coincidence events falling into an energy window of 511 keV × (1 ± energy resolution (%)/100) were used for the time resolution measurement. We employed spline interpolation in factors of 10 for each pulse to more precisely measure the pulse arrival time. To determine the best time pickoff method, we digitally implemented a leading edge discriminator (LED) and constant fraction discriminator (CFD) with varying thresholds. The LED used a certain fraction of the averaged 511 keV pulse amplitude as a time pickoff point, whereas the CFD used a certain fraction of each pulse amplitude. Threshold levels of 1–30% were applied for both the LED and CFD. The coincidence resolving time (CRT) was estimated as the FWHM of the Gaussian fitted histogram of the arrival time difference between the test and reference PMTs. The single time resolution of the test PMT was calculated as $\sqrt{\mathrm{CRT}^2 - \Delta t_{\mathrm{ref}}^2}$, where Δt_{ref} corresponds to the time resolution of the reference PMT. The relative output pulse was measured during testing of the additional coupling positions of the crystals, being defined as the percentage of the pulse amplitude relative to the center position configuration.

3. Results

3.1. Pulse properties

A narrow energy window of 1% for 511 keV pulses was applied to investigate the properties of the PMT output pulse signals. Sampled signals of both PMTs are shown in figure 3(a). The pulse amplitude was proportional to the intrinsic gain, which can be presented as a product of the luminous sensitivity ratio and blue sensitivity (Hamamatsu Photonics K. K. Editorial Committee 2007) (figure 3(b)) . The average amplitude of R13478 was 47% of that of R9800 at the recommended supply voltages (1500 and 1300 V for R13478 and R9800, respectively). The amplitude increased exponentially with increased supply voltage (figure 3(c)). The pulse rise time was evaluated as the time interval corresponding to the 10–90% range of the pulse amplitude at the rising edge. The averages and standard deviations of rise time of R13478 and R9800 were 1.54 ± 0.02 ns and 1.64 ± 0.01 ns, respectively (P-value < 0.005).

3.2. Energy and time resolutions of PMTs

Figure 4 shows the main performance results for both PMTs, i.e. histograms of the measured coincidence time difference and energy. The best average single time resolutions of R13478 and R9800 at the recommended supply

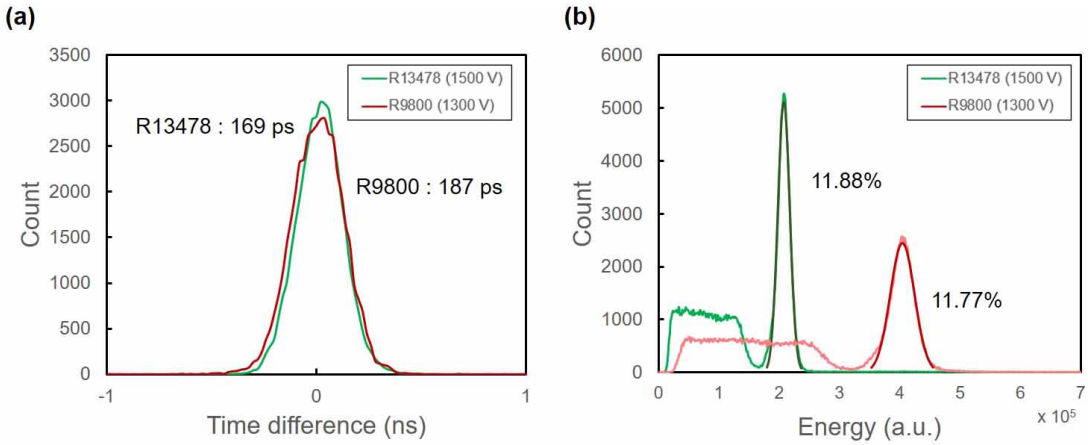

Figure 4. (a) Coincidence time difference and (b) energy histograms of R13478 and R9800 for recommended supply voltages.

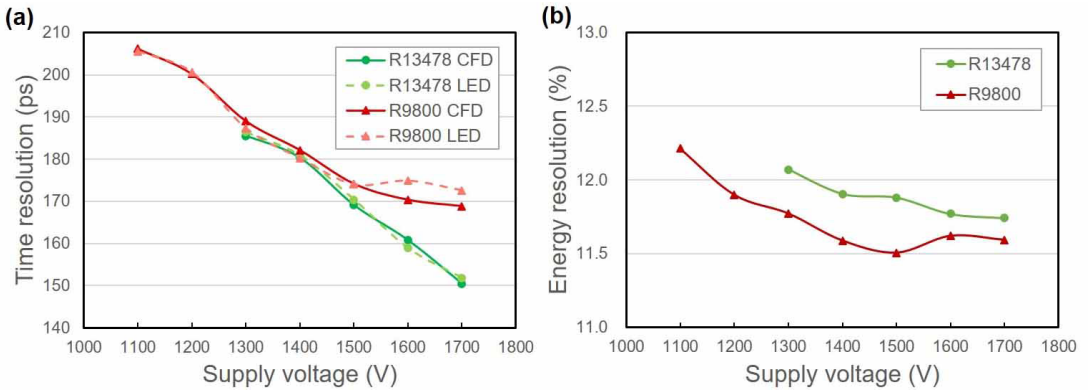

Figure 5. (a) Single time resolution and (b) energy resolution dependence on supply voltages. An interactive version of this figure is available.

voltages were 169 ± 4.56 ps and 187 ± 4.17 ps, respectively (P-value < 0.01). The energy resolutions were 11.88 ± 0.60% and 11.77 ± 0.25% for R13478 and R9800, respectively.

The time resolution dependence on supply voltage for R13478 and R9800 is compared in figure 5(a). It is apparent that higher supply voltage yields better time resolution, which is because of the higher gain. Both PMTs exhibited comparable time resolutions when the same supply voltages lower than 1500 V were applied. However, for supply voltages higher than 1500 V, R13478 exhibited notably better time resolution than R9800. As the supply voltage increased, the energy resolution improved slightly because the uncertainties of the estimated radiation energy decreased with increasing gain (figure 5(b)).

The thresholds at which the best time resolutions were obtained were 3% and 10% for R13478 and R9800, respectively (figure 6). The common trend for the time resolution was to degrade as time pickoff threshold increased because of the time-walk effect. Further, the time resolution degraded at a very low threshold level because of the noise and time jitter of the photoelectrons (Derenzo *et al* 2014). From comparison of time pickoff methods, the CFD tended to yield better time resolution than the LED at high thresholds; this is because the CFD is more robust to the time-walk effect caused by fluctuation of the pulse amplitudes.

3.3. Performance dependence on crystal position

As apparent from the results listed in table 2, when the crystal was coupled to the edge of the PMT window, the pulse amplitude decreased to approximately 75%. This degradation occurred because of the relatively low quantum efficiency of the photocathode and photoelectron collection efficiency at the edge. These decreased pulse amplitudes in turn induced degradation of both the energy and time performance.

The amplitudes of the output pulses from the laid crystal were approximately 30% larger than those from the center-positioned crystal. For the laid crystal setup, the scintillation light traverses a shorter distance inside the crystal before arriving at the PMT window and there is less chance of self-absorption, scattering or escape for this light. Therefore, the time resolution was improved with increased outputs for both PMTs. The time resolutions for the laid crystal setup of R13478 and R9800 were 144 ± 3.42 ps and 167 ± 3.11 ps, respectively (P-value < 0.005). Although, for R13478, the degradation of the timing resolution from the center to the edge

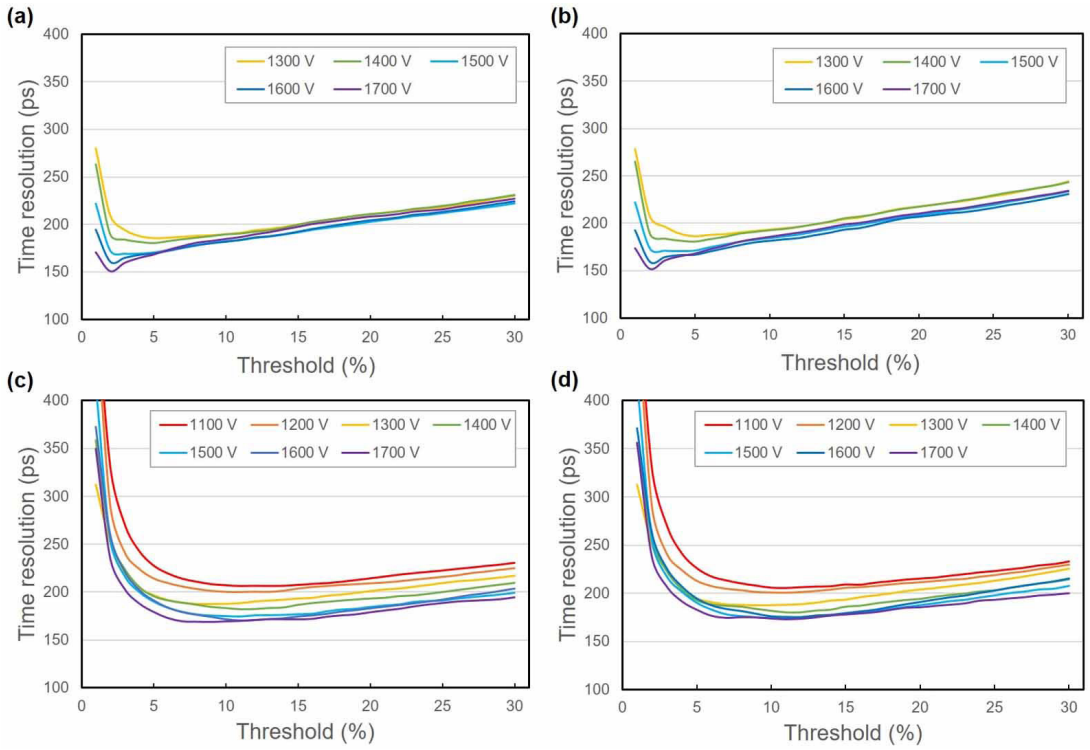

Figure 6. Time resolution dependence on time pickoff method and supply voltage. (a) R13478 CFD, (b) R13478 LED, (c) R9800 CFD, and (d) R9800 LED. An interactive version of this figure is available.

Table 2. Output pulse, energy resolution and time resolution dependence on crystal position.

PMT (supply voltage)		R13478 (1500 V)	R9800 (1300 V)
Edge	Output pulse (%)	78.40	74.56
	Energy resolution (%)	12.20	12.08
	Time resolution (ps)	204.7	210.0
Laid	Output pulse (%)	129.9	126.2
	Energy resolution (%)	12.10	12.31
	Time resolution (ps)	143.6	166.5

is slightly larger than R9800, the improvement of the timing resolution for the laid position as compared to the center position is larger in R13478. This implies that the timing uncertainty caused by the spatial difference of photoelectron emission position was smaller in R13478 than in R9800.

4. Discussion

One of the most significant differences between R13478 and R9800 was in the time resolution at a low time pickoff threshold. It is well known that time jitter generated within a photodetector is critical to the timing precision of early-arrival photoelectrons (Derenzo *et al* 2014, Hyman 1965). Under ideal conditions for which time jitter is zero, the jitter of a single photoelectron pulse is the smallest for the first photoelectron and increases proportionally to the square root of the order of arrived photoelectrons. However, as jitter increases, the leading-edge trigger level becomes optimal for a higher-order number of photoelectrons. Consequently, the better time resolution of R13478 compared to R9800 at a low time pickoff threshold can be explained by considering the effects of the accelerating node on the transit time jitter reduction. In the configuration with the crystal coupled to the small area in the center of the PMT window, the factor σ_1^2 mentioned in section 1 dominates time jitter σ_{PMT} as the effects of the spatial transit time difference can be neglected. In addition, the low intrinsic dark current of R13478 also contributed to this result. When a very low threshold was applied, time pickoff accuracy is degraded by noise near the rising parts of the pulses.

To verify the effects of the accelerating electrode on the alleviation of the photoelectron emission position dependence, we coupled crystals to the PMTs in the laid position, so that electrons were emitted from a wider area in coincidence. Significant improvement in the time resolution was measured for the laid crystal position,

indicating reduction of σ_2^2. By applying a strong electric field at the edges of the PMTs, photoelectrons emitted from the edges were collected efficiently. These effects are expected to improve the time performance for several system configurations, such as light-sharing PET block detectors with round PMTs (Berg *et al* 2016, Peng *et al* 2015).

Another important difference was the time resolution at high supply voltage, which resulted from the dark current. Compared to R9800, R13478 has an obviously small anode dark current (table 1). With increased supply voltage, both the gain and anode dark current increase. The dark current increases even more quickly under an extremely high supply voltage mainly because of field emission, which is emission of electron from the dynodes induced by a very strong electric field (Hamamatsu 2007). This noise causes uncertainty in the time pickoff, which eventually degrades the time resolution.

Although R13478 and R9800 have different properties with regard to gain, recommended supply voltage, and noise, we have demonstrated the effects of the accelerating electrode and the reduced transit time jitter of the new PMT, R13478. Further development of the transit time jitter reduction technique will yield meaningful improvement in the time performance of PMTs.

5. Summary and conclusion

In this study, the time performance of the accelerating-electrode-containing R13478 PMT was compared against that of the existing R9800 PMT. R13478 PMT exhibited excellent time performances with the time resolution of 169 ps when coupled to the LGSO crystal. Significant improvement in time resolution was observed for a low time pickoff threshold and laid crystal position, indicating reduction of the transit time and harmonization of the spatial transit time difference. These are both critical components influencing the overall transit time jitter of PMT. The results obtained in this study verify the important role of the accelerating electrode which is a new feature of R13478 PMT. In addition, the better time performance of R13478 in extremely high supply voltages confirmed its excellent noise properties. Accordingly, we can conclude that the transit time jitter reduction by equipping an accelerating electrode effectively improves time performance of PMT which would be suitable for fast timing applications.

Acknowledgments

This work was supported by grants from the National Research Foundation of Korea (NRF) funded by the Korean Ministry of Science and ICT (Grant Nos. NRF-2014M3C7034000 and NRF-2016R1A2B3014645). We thank K Watase and T Ichikawa (Hamamatsu Photonics K. K.) for useful discussions on the newly provided PMT. We also thank C S Levin and J W Cates (Stanford University) for providing us LGSO crystals.

ORCID iDs

Jae Sung Lee https://orcid.org/0000-0001-7623-053X

References

Adamo G, Parisi A, Stivala S, Tomasino A, Agrò D, Curcio L, Giaconia G C, Busacca A and Fallica G 2014 Silicon photomultipliers signal-to-noise ratio in the continuous wave regime *IEEE J. Sel. Top. Quant.* **20** 284–90

Berg E and Roncali E, Kapusta M, Du J and Cherry S R 2016 A combined time-of-flight and depth-of-interaction detector for total-body positron emission tomography *Med. Phys.* **43** 939–50

Cates J W and Levin C S 2016 Advances in coincidence time resolution for PET *Phys. Med. Biol.* **61** 2255–64

Conti M 2011a Focus on time-of-flight PET: the benefits of improved time resolution *Eur. J. Nucl. Med. Mol. Imaging* **38** 1147–57

Conti M 2011b Improving time resolution in time-of-flight PET *Nucl. Instrum. Methods Phys. Res.* A **648** S194–8

Derenzo S E, Choong W-S and Moses W W 2014 Fundamental limits of scintillation detector timing precision *Phys. Med. Biol.* **59** 3261–86

El Fakhri G, Surti S, Trott C M, Scheuermann J and Karp J S 2011 Improvement in lesion detection with whole-body oncologic time-of-flight PET *J. Nucl. Med.* **52** 347–53

Hamamatsu Photonics K. K. Editorial Committee 2007 *Photomultiplier Tubes—Basics and Applications* 3th edn (Hamamatsu: Hamamatsu Photonics K. K. Electron Tube Division) pp 67–71

Hyman L G 1965 Time resolution of photomultiplier systems *Rev. Sci. Instrum.* **36** 193–6

Ito M, Lee J P and Lee J S 2013 Timing performance study of new fast PMTs with LYSO for time-of-flight PET *IEEE Trans. Nucl. Sci.* **60** 30–7

Karp J S, Surti S, Daube-Witherspoon M E and Muehllehner G 2008 Benefit of time-of-flight in PET: experimental and clinical results *J. Nucl. Med.* **49** 462–70

Ko G B and Lee J S 2015 Performance characterization of high quantum efficiency metal package photomultiplier tubes for time-of-flight and high-resolution PET applications *Med. Phys.* **42** 510–20

Krishnamoorthy S, LeGeyt B, Werner M E, Kaul M, Newcomer F M, Karp J S and Surti S 2014 Design and performance of a high spatial resolution, time-of-flight PET detector *IEEE Trans. Nucl. Sci.* **61** 1092–8

Moses W W 2007 Recent advances and future advances in time-of-flight PET *Nucl. Instrum. Methods Phys. Res.* A **580** 919–24

Moses W W and Ullisch M 2006 Factors influencing timing resolution in a commercial LSO PET camera *IEEE Trans. Nucl. Sci.* **53** 78–85

Moszyński M and Vacher J 1977 Influence of incident light wavelength on time jitter of fast photomultipliers *Nucl. Instrum. Methods Phys. Res.* A **141** 319–23

Mullani N A, Ficke D C, Hartz R, Markham J and Wong G 1981 System design of fast PET scanners utilizing time-of-flight *IEEE Trans. Nucl. Sci.* **28** 104–8

Peng Q, Choong W-S, Vu C, Huber J S, Janecek M, Wilson D, Huesman R H, Qi J, Zhou J and Moses W W 2015 Performance of the Tachyon time-of-flight PET camera *IEEE Trans. Nucl. Sci.* **62** 111–9

Son J-W, Ko G B, Won J Y, Yoon H S and Lee J S 2016 Development and performance evaluation of a time-of-flight positron emission tomography detector based on a high-quantum-efficiency multi-anode photomultiplier tube *IEEE Trans. Nucl. Sci.* **63** 44–51

Szczesniak T, Moszynski M, Swiderski L, Nassalski A, Lavoute P and Kapusta M 2007 Fast photomultipliers for TOF PET *IEEE NSS Conf. Rec.* **4** 2651–9

Tomitani T 1981 Image reconstruction and noise evaluation in photon time-of-flight assisted positron emission tomography *IEEE Trans. Nucl. Sci.* **28** 4581–9